MOLECULAR IMAGING AND BIOLOGY

RESEARCH ARTICLE

Molecular Imaging of the Translocator Protein (TSPO) in a Pre-Clinical Model of Breast Cancer

Shelby K. Wyatt,[1,2] H. Charles Manning,[1,2,3,4,5,6] Mingfeng Bai,[7] Stephanie N. Bailey,[7] Pascal Gallant,[8] Guobin Ma,[8] Laura McIntosh,[8] Darryl J. Bornhop[1,6,7,9]

[1]Vanderbilt University Institute of Imaging Science (VUIIS), Vanderbilt University Medical Center, Nashville, TN, USA
[2]Department of Radiology and Radiological Sciences, Vanderbilt University Medical Center, Nashville, TN, USA
[3]Department of Biomedical Engineering, Vanderbilt University, Nashville, TN, USA
[4]Department of Neurological Surgery, Vanderbilt University Medical Center, Nashville, TN, USA
[5]Chemical and Physical Biology Program, Vanderbilt University, Nashville, TN, USA
[6]The Vanderbilt-Ingram Cancer Center, Vanderbilt University Medical Center, Nashville, TN, USA
[7]Department of Chemistry, Vanderbilt University, Nashville, TN, USA
[8]ART Advanced Research Technologies Inc., Montreal, Quebec, Canada
[9]The Vanderbilt Institute for Chemical Biology, Vanderbilt University, Nashville, TN, USA

Abstract

Purpose: To quantitatively evaluate the utility of a translocator protein (TSPO)-targeted near-infrared (NIR) probe (NIR-conPK11195) for *in vivo* molecular imaging of TSPO in breast cancer.
Procedures: NIR-conPK11195 uptake and TSPO-specificity were validated in TSPO-expressing human breast adenocarcinoma cells (MDA-MB-231). *In vivo* NIR-conPK11195 biodistribution and accumulation were quantitatively evaluated in athymic nude mice bearing MDA-MB-231 xenografts.
Results: Fluorescence micrographs illustrated intracellular labeling of MDA-MB-231 cells by NIR-conPK11195. Quantitative uptake and competition assays demonstrated dose-dependent ($p<0.001$) and TSPO-specific ($p<0.001$) NIR-conPK11195 uptake. *In vivo*, NIR-conPK11195 preferentially labeled MDA-MB-231 tumors with an 11-fold ($p<0.001$) and 7-fold ($p<0.001$) contrast enhancement over normal tissue and unconjugated NIR dye, respectively.
Conclusions: NIR-conPK11195 appears to be a promising TSPO-targeted molecular imaging agent for visualization and quantification of breast cancer cells *in vivo*. This research represents the first study to demonstrate the feasibility of TSPO imaging as an alternative breast cancer imaging approach.

Key words: Peripheral benzodiazepine receptor, Translocator protein, PK 11195, Molecular imaging, Breast cancer, MDA-MB-231, Diagnosis, Steroidogenesis, Prognosis, Staging

Significance: This is the first study to demonstrate the feasibility of molecular imaging of the translocator protein (TSPO), previously termed the peripheral benzodiazepine receptor, as a potential approach to breast cancer imaging. The TSPO represents an attractive target for molecular imaging of disease due to its overexpression in a variety of neurological disorders and cancers, including breast cancer, as well as its correlation with disease stage and clinical prognosis.

We demonstrate that a near-infrared (NIR) TSPO-targeted probe developed in our laboratory (NIR-conPK11195) selectively labels *in vivo* breast cancer cells in a pre-clinical model of human breast adenocarcinoma (MDA-MB-231). NIR-conPK11195 exhibits significant dose-dependent cellular uptake and TSPO-specificity in *in vitro* MDA-MB-231 cells ($p<0.001$). *In vivo*, NIR-conPK11195 preferential labels MDA-MB-231 tumors with an 11-fold contrast enhancement over normal tissue and a 7-fold improvement in fluorescence signal with respect to free (unconjugated) NIR dye ($p<0.001$). Given the importance of molecular imaging in cancer detection, diagnosis, and monitoring of disease as well as the impact of pre-clinical studies on therapeutic efficacy monitoring and drug discovery, we believe the utility of NIR-conPK11195 for molecular imaging of TSPO in breast cancer will be of considerable interest to both the molecular imaging and cancer research communities. Furthermore, this work represents a potentially translational methodology as radiolabeled PK 11195 has already been used in the clinic for imaging of neurodegenerative diseases and gliomas.

Correspondence to: Darryl J. Bornhop; *e-mail:* darryl.bornhop@vanderbilt.edu

Introduction

Breast cancer is the second most frequently diagnosed cancer in women and the second most common cancer type responsible for women's deaths [1]. In 2009, the American Cancer Society estimated that 192,370 women and 1,910 men would be newly diagnosed with invasive breast cancer in the United States alone, while another 40,170 women and 440 men were expected to die from breast cancer [1]. The 5-year survival rate of breast cancer patients is 84% once the cancer has spread regionally, declining to 27% in patients with distant or metastatic disease. However, the 5-year survival rate surpasses 95% if breast cancer is detected in its initial stages [1]. Thus, breast cancer mortality rates could be significantly influenced by the development of improved detection and diagnosis techniques.

Currently, imaging plays a major role in the early detection and characterization of breast cancer. Conventional X-ray mammography is the most common breast cancer screening technique and has shown superiority to self-examination alone for detecting breast cancer lesions [2]. However, standard X-ray mammography requires the use of harmful ionizing radiation and its sensitivity is limited in patient populations with dense breast tissue such as in younger women and women on hormone replacement therapies [3]. In addition, X-ray mammography is an anatomical imaging technique that relies solely on morphological changes rather than cellular and molecular events and often cannot distinguish between benign and malignant lesions. Consequently, more sophisticated imaging approaches and/or invasive biopsy procedures are often required to further characterize the suspect tissue.

Several alternative breast cancer imaging approaches have been evaluated, including dynamic contrast-enhanced magnetic resonance imaging (DCE-MRI), ultrasound, and optical imaging. In women with inherited breast cancer susceptibility, DCE-MRI appears to have greater sensitivity than X-ray mammography and ultrasound [2, 4]. However, DCE-MRI is limited by its high cost and long imaging times and suffers from lower specificity and more variable interpretations than X-ray mammography [2, 4]. Conversely, ultrasound has been shown to play a pivotal role in the discrimination between benign and malignant lesions in breast cancer screening, but is limited by the difficulties in image interpretation and the inability to consistently detect and identify microcalcifications [2, 5]. Optical mammography systems are also being developed that capitalize on either intrinsic or extrinsic contrast mechanisms [6–12]. Although photon penetration in deep tissues and three-dimensional probe localization remain a challenge for optical imaging, the use of near-infrared (NIR) mammography may prove beneficial in the near future [13–15].

Molecular imaging using positron emission tomography (PET) probes has also been investigated in breast cancer imaging; common tracers include 2-[^{18}F]fluoro-2-deoxy-glucose ([^{18}F]FDG) to assess glucose metabolism [16–19], 3′-[^{18}F]fluoro-3′-deoxythymidine ([^{18}F]FLT) to measure thymidine kinase I activity [20–23] and [^{18}F]-16-α-17-β-fluoroestradiol ([^{18}F]FES) to evaluate estrogen receptor expression [24–26]. Several groups have demonstrated success with these agents in the management of breast cancer patients, particularly for assessing the extent and stage of the disease as well as for monitoring treatment response (reviewed in: [26–29]). Molecular imaging strategies such as these are advantageous over anatomical imaging techniques as they enable evaluation of physiological processes that may precede morphological or physical changes. Further development of novel molecular imaging techniques for breast cancer imaging would provide additional and potentially more specific information regarding the biological characteristics of the suspicious lesion, particularly in cases where treatment options may be targeted to other cellular processes. For these techniques to succeed, non-toxic agents with high *in vivo* specificity and the ability to report physiology must be developed.

Towards this goal, we have developed a molecular imaging agent that targets the translocator protein (TSPO [30]), previously termed the peripheral benzodiazepine receptor (PBR), and evaluated its use for *in vivo* molecular imaging of breast cancer. The TSPO is a transmitochondrial and nuclear membrane protein that is involved in a number of cellular processes including steroidogenesis, cholesterol transport, cellular proliferation, and apoptosis [30]. Although TSPO is naturally expressed at various levels in normal tissue, TSPO has been shown to be highly upregulated in a variety of neurodegenerative diseases and cancers, including breast cancer [30–37]. The expression profile of TSPO even appears to correlate with aggressive phenotype [33] and *in vivo* tumor growth [34]. Clinically, TSPO expression has been shown to be a potential predictor of poor prognosis [35]. Taken together, these observations indicate that TSPO-targeted molecular imaging agents may have utility in the evaluation and characterization of breast cancer.

Previously, we reported the use of the TSPO-targeted NIR probe developed in our laboratory (NIR-conPK11195) for non-invasive detection of primary colonic tumors arising in Smad3$^{-/-}$ mice [38]. In this study, we aimed to validate the TSPO-specificity of NIR-conPK11195 *in vitro* and to subsequently translate the use of this probe from *in vitro* breast cancer cell labeling to *in vivo* imaging of TSPO in a highly relevant pre-clinical breast cancer model. Specifically, these studies were conducted in MDA-MB-231 human breast adenocarcinoma xenografts, a very common and widely used mouse model of human breast cancer, particularly for studying aggressive phenotypes. The intracellular labeling of TSPO-expressing MDA-MB-231 cells were first visualized by fluorescence microscopy. The dose-dependency and TSPO-specificity of NIR-conPK11195 were then evaluated in *in vitro* cellular uptake and competitive binding assays. Subsequently, the *in vivo* biodistribution and tumor-specific accumulation of NIR-conPK11195 were quantitatively assessed and compared with that of the free (unconjugated) NIR dye in MDA-MB-231 xenografts grown on athymic

nude mice. The results presented here suggest that NIR-conPK11195 is a promising TSPO-targeted molecular imaging agent for visualization and quantification of breast cancer cells *in vivo* and represents the first study to demonstrate the feasibility of TSPO imaging as an alternative breast cancer imaging approach.

Materials and Methods

Materials

The IRDye™ 800CW NHS Ester dye and IRDye™ 800-acid (designated here as "free NIR dye") were obtained from LI-COR Biosciences (Lincoln, NE). Dimethylsulfoxide (DMSO) was purchased from Fisher Scientific (Pittsburgh, PA). MDA-MB-231 cells were acquired from the American Type Culture Collection (ATCC; Manassas, VA). Calcium- and magnesium-free phosphate buffered saline (CMF-PBS), fetal bovine serum (FBS), and Leibovitz's L-15 media supplemented with 2 mM L-glutamine were obtained from Invitrogen Corporation (Carlsbad, CA). PK 11195 was purchased from Sigma Aldrich (St. Louis, MI). Female BALB/c immunodeficient mice (8–9 weeks of age and weighing 15–20 g) were obtained from Charles River Canada Inc. (Lasalle, St-Constant, Quebec).

Synthesis and Characterization of NIR-conPK11195

NIR-conPK11195 was synthesized as previously described [38] by coupling the IRDye™ 800CW NHS ester dye to the conjugable form of PK 11195 developed in our laboratory (conPK11195; [39]). Briefly, IRDye™ 800CW NHS ester (2 mg, 1.7 μmol) and conPK11195 (2.5 mg, 6.6 μmol) were mixed in DMSO (5 mL) in a round bottom flask and stirred under argon flow for 1 h. The reaction was monitored using high-performance liquid chromatography (HPLC) analysis on a Varian Polaris C-18 column (250×4.6 mm) at a flow rate of 0.8 mL/min. Flow A was 20 mM tetrabutylammonium bromide in water and flow B was 20 mM tetrabutylammonium bromide in 90% acetonitrile and 10% water. The elution method for analytical HPLC started with a linear gradient from 100% to 50% A over 10 min, held at 50% A for 5 min, arrived at 10% A in another 10 min, held at 10% A for 10 min, and finally returned to 100% A over 2 min. The elution profile was monitored by absorbance at 254 (unreacted conPK11195) and 780 nm. Product was purified by preparative HPLC using a Varian Polaris C-18 column (250× 21.2 mm) at 17 mL/min. The collected solution was concentrated by vacuum rotary evaporation, frozen to −78ºC and dried under a freeze-dry system. The collected green solid was dissolved in DMSO, and the residual tetrabutylammonium bromide was removed by centrifugation. The amount of NIR-conPK11195 was determined by absorption in DMSO solution at 797 nm (0.6 mg, 24%). Note: The $\lambda_{ex,max}$ is 797 nm in DMSO and $\lambda_{ex,max}$ is 777 nm in CMF-PBS.

MS (ESI)$^+$ [M+H]$^+$ calcd 1,366.4, found 1,366.3. ^{1}H NMR 500 MHz (MeOD) δ 8.55 (s, 1H), 8.10 (d, *J*=8.0 Hz, 1H), 7.97–7.89 (m, 2H), 7.85–7.77 (m, 7H), 7.67–7.46 (m, 7H), 7.33 (d, *J*=8.5 Hz, 1H), 7.24 (d, *J*=8.5 Hz, 1H), 7.15 (d, *J*=8.5 Hz, 2H), 6.25 (d, *J*=14.0 Hz, 1H), 6.14 (d, *J*=14.0 Hz, 1H), 4.15–4.10 (m, 2H), 4.08–4.04 (m, 2H), 3.44 (t, *J*=7.0 Hz, 2H), 3.17 (q, *J*=2.5 Hz, 5H), 3.12 (t, *J*=2.0 Hz, 2H), 3.01 (q, *J*=2.5 Hz, 5H), 2.89–2.85 (m, 2H), 2.77–2.69 (m, 4H), 2.15 (t, *J*=2.0 Hz, 2H), 2.03–2.00(m, 2H), 1.94–1.90 (m, 6H), 1.79–1.75 (m, 2H), 1.67–1.63 (m, 5H), 1.49–1.46 (m, 2H), 1.37 (d, *J*=4.5 Hz, 7H).

For spectroscopic characterization, the absorbance spectra of free NIR dye and NIR-conPK11195 were measured using a Shimadzu UV-VIS 1700 spectrophotometer (Columbia, MD) and the emission spectra were measured using a PTI Technologies spectrofluorometer (Oxnard, CA).

Cell Culture

The TSPO-expressing, human metastatic breast adenocarcinoma cell line (MDA-MB-231) was propagated in Leibovitz's L-15 medium supplemented with 2 mM L-glutamine, 10% FBS, and 1% penicillin-streptomycin or 50 mg gentamicin in seal plug culture flasks (Corning; Corning, NY) at 37°C and 95% humidity. The medium was replaced every three days or as necessary. After attaining confluence, the cells were sub-cultured approximately 1:2 to 1:10.

In Vitro Fluorescence Microscopy

MDA-MB-231 cells (~100,000) were plated in parafilm-wrapped, collagen-coated glass bottom dishes (MatTek Corporation; Ashland, MA) 48 h prior to experimentation. The cells were first washed once with warmed FBS-free medium and then incubated with 10 μM NIR-conPK11195 or 10 μM free NIR dye for 30 min at 37°C. Subsequently, the cells were washed three times with CMF-PBS. A Nikon Eclipse TE2000-U fluorescence microscope equipped with a mercury lamp, indocyanine green filter set and a Hamamatsu ORCA II BT 512 camera controlled by Metamorph v6.1 (Molecular Devices Corporation; Downingtown, PA) was used for imaging.

In Vitro Uptake and Competition Studies

MDA-MB-231 cells were plated at 10,000 cells per well in parafilm-wrapped 96 MicroWell™ Nunclon™Δ Optical Bottom Plates (Nalge Nunc International; Rochester, NY) and incubated under standard culture conditions for approximately 48 h. Immediately prior to experimentation, the cells were washed once with 37°C FBS-free medium to remove any dead cells and serum. The cells were then divided into four populations and evaluated in triplicate: (1) cells incubated with increasing concentrations of NIR-conPK11195 (1, 4, 7, 10, 40, 70, 100, 400, 700 nM, 1 μM) in FBS-free medium (100 μL volume), (2) cells simultaneously incubated with the same concentrations of NIR-conPK11195 and 100 μM PK 11195, (3) cells incubated with the same concentrations of free NIR dye, and (4) undosed cells as blanks. Following a 30-min incubation, the cells were gently washed twice with FBS-free medium and imaged on the Odyssey Infrared Imaging System (LI-COR Biosciences; Lincoln, NE) at 169 μm resolution, 3 mm focus offset, and 4.0, 8.0, and 10.0 intensity (gain) in the 800 nm channel. The average raw fluorescence intensity of each population ± standard deviation was then plotted in terms of NIR-conPK11195 or free NIR dye concentration; *n*=3. The percent change in raw fluorescence intensity due to PK 11195 competition was calculated as $\frac{FI_{blocked}-FI_{unblocked}}{FI_{unblocked}}*100$ where FI is raw fluorescence intensity.

Murine Model: Cell Implantation and Tumor Growth

The *in vivo* imaging studies were performed at LAB Pre-Clinical Research International Inc. (Montreal, Canada) under approved LAB protocols.

MDA-MB-231 cells were propagated until near confluency as described above. Cells were harvested by incubation with trypsin, pelleted by centrifugation, resuspended in sterile CMF-PBS, counted and assessed for viability (percent) using trypan blue staining. The cells were again pelleted by centrifugation, resuspended in sterile CMF-PBS at a concentration of 5×10^6 cells/100 μL and kept on ice. Prior to cell implantation, the cell-containing tube was gently inverted several times to assure homogenous cell distribution. Female BALB/c immunodeficient mice were injected with 5×10^6 MDA-MB-231 cells (100 μL volume) subcutaneously at the level of the right scapula.

In Vivo Imaging Studies

After approximately 3 weeks of tumor growth, the MDA-MB-231 tumor bearing mice were injected with four nanomoles of either free NIR dye or NIR-conPK11195 in sterile saline via the tail vein (100 μL volume). The biodistribution and accumulation of the free NIR dye and TSPO-targeted probe were monitored in real time using the Optix® pre-clinical optical molecular imager (ART Advanced Research Technologies Inc., Montreal, Quebec [40]) equipped with an excitation laser at 780 nm and an 825 nm long-pass emission filter (Barr Associates; Westford, MA). Fluorescence signal was recorded using a photomultiplier tube (Hamamatsu) coupled to time-correlated single photon counting system (Becker & Hickl, Berlin, German). Images were obtained preinjection and approximately 10 min, 1, 4, 6, 12, 18, 24, and 48 h post-injection. Approximately 48 h post-injection, the mice were euthanized and tissues were harvested (kidneys, liver, brain, and tumors), imaged, and fixed in 10% formalin. The fixed tumors were then paraffin embedded, sliced, and stained with hematoxylin and eosin (H & E) for histological characterization.

During the imaging sessions, the mice were kept on a heated animal support plate under general anesthesia by inhalation of 2.5% isoflurane. All animals were supplied with Tears Naturale P.M. (Alcon, Mississauga, ON).

Throughout the study, the scanning step size, or spatial resolution, was maintained at 1.5 mm. The excitation laser power (40–800 μW) and fluorescence signal integration time (250 ms–1 s) were optimized at each individual time point using the peak value of the temporal point-spread function (TPSF) to maximize the signal and avoid saturation of the detector. Thus, the fluorescence intensity was subsequently normalized to laser power and integration time to allow for direct comparison between mice and over time. For visualization purposes, images were smoothed using a linear interpolation algorithm in the OptiView™ analysis software (ART Advanced Research Technologies, Inc).

The data were processed using a customized package provided by ART, which allows specific regions of interest (ROIs) to be manually defined and quantified in terms of normalized integrated TPSF intensity. Since these tumors were subcutaneous, the effects of light propagation were approximately the same for all cases and the fluorescence intensity may be used as a quantification indicator. ROIs of equivalent size (9 mm×6 mm) were drawn around the tumor itself and the opposite hind limb, defined as "normal" tissue. The average normalized integrated TPSF intensities (±standard deviation) for each group were then plotted as a function of time post-injection to generate time activity curves and monitor pharmacokinetics. To further determine tumor specificity, we compared the tumor intensities with the normal tissue intensities in mice that were injected with NIR-conPK11195 (tumor/normal). We also compared the tumor intensities in the mice injected with NIR-conPK11195 with the tumor intensities of mice injected with free NIR dye (targeted/free).

Statistical Analysis

Statistical significance was determined using a one-way analysis of variance test and the Holm–Sidak method for pairwise multiple comparisons with an overall significance level of 0.05 (SigmaStat v3.10).

Results

The TSPO-targeted NIR molecular imaging agent, NIR-conPK11195, was synthesized by coupling the IRDye™ 800CW NHS Ester dye to the primary amine on the conjugable PK 11195 analog (conPK11195, [39]) previously developed in our laboratory and purified by preparative HPLC (Fig. 1a, b). In CMF-PBS, NIR-conPK11195 exhibits an absorbance maximum centered at 777 nm with peak emission at 799 nm (λ_{ex}=777 nm; Fig. 1c). This spectroscopic profile is very similar to that of the IRDye™ 800-acid (designated here as "free NIR dye", λ_{abs}=774 nm and λ_{em}=796 nm). The absorbance and fluorescence spectra for NIR-conPK11195 are red shifted by only 3 nm relative to the free NIR dye and the Stokes shift is 22 nm for both compounds, suggesting that the spectroscopic properties of IRDye™ 800CW were not substantially altered by the conjugation of conPK11195. Furthermore, the NIR-conPK11195 spectroscopy falls directly within the NIR tissue transparency window and thus overcomes some of the major limitations of other fluorescently-labeled TSPO-targeted agents when used *in vivo* [39, 41–45].

To visualize cellular uptake of NIR-conPK11195 in comparison to free NIR dye, fluorescence microscopy was performed in live TSPO-expressing, human metastatic breast adenocarcinoma (MDA-MB-231) cells. The fluorescence micrograph in Fig. 2a illustrates appreciable fluorescence and cellular uptake of NIR-conPK11195. Using the same experimental conditions, instrument settings, and grayscale dynamic range, the cells incubated with free NIR dye exhibit discernibly less fluorescence signal (Fig. 2b). In addition, the fluorescence overlay in Fig. 2a provides evidence that the NIR signal is emanating from the nuclear and perinuclear region of the NIR-conPK11195 dosed cells, as one would expect from the nuclear and mitochondrial location of TSPO in MDA-MB-231 cells [33].
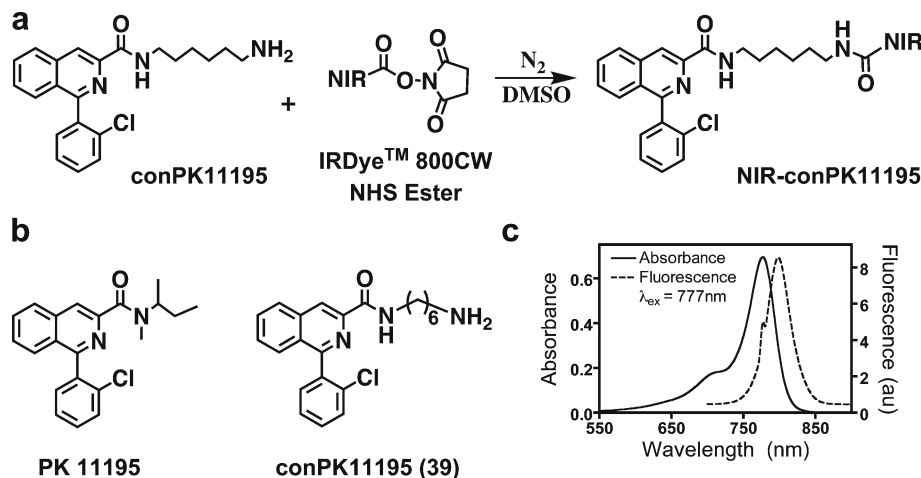
Fig. 1. **a** Synthetic pathway, **b** relevant chemical structures, and **c** spectroscopic properties of NIR-conPK11195 in CMF-PBS (λ_{ex}=777 nm).

To further evaluate the cellular uptake and TSPO labeling specificity of NIR-conPK11195, competitive binding assays were performed in a multiwell plate format. Fig. 3 illustrates the significant (28-fold overall) increase in fluorescence intensity as a function of increasing NIR-conPK11195 concentration from 1 to 70 nM ($p<0.001$; circle). It is unlikely that the observed dose-dependent uptake is actually due to non-specific binding since the cells dosed with the non-targeted, free NIR dye (square) show significantly less fluorescence signal than those cells that were incubated with NIR-conPK11195 at each concentration ($p<0.001$). In fact, the

cells dosed with free NIR dye remain statistically indistinguishable from the undosed blanks (diamond). Combined, these results suggest that the cellular uptake of NIR-conPK11195 is conPK11195-specific. In addition, the significant (33–88%) attenuation of the fluorescence intensity due to the presence of the traditional PK 11195 ligand ($p<0.001$; inverted triangle) provides evidence for TSPO-specificity.

Although the competition assay included concentrations ranging from 1 nM to 1 µM, the dynamic range of the Odyssey Infrared Imaging System restricted the quantification of this assay to two orders of magnitude in incubation
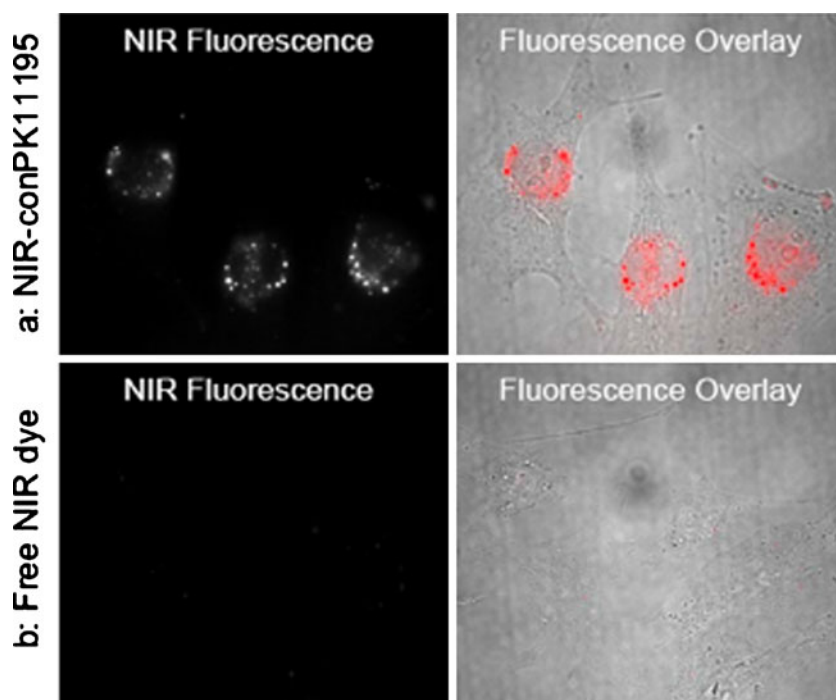

Fig. 2. Live cell fluorescence microscopy illustrates appreciable NIR fluorescence and cellular uptake of NIR-conPK11195 (**a**), but not free NIR dye (**b**). MDA-MB-231 cells were incubated with 10 µM NIR-conPK11195 (**a**) or free NIR dye (**b**) for 30 min at 37°C in FBS-free medium. Pseudocolored fluorescence images overlaid onto the corresponding white light images also provide evidence of nuclear and perinuclear localization of NIR-conPK11195.
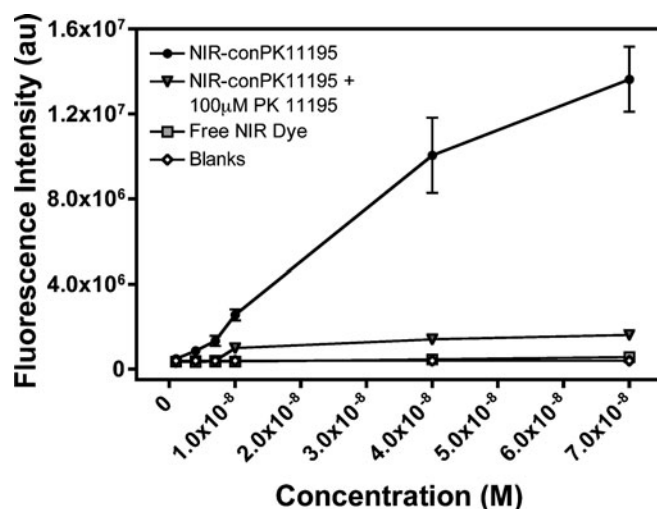
Fig. 3. Cellular uptake and competition assays indicate significant dose dependent ($p < 0.001$) and TSPO-specific ($p < 0.001$) cellular uptake of NIR-conPK11195. The average fluorescence intensity per well±standard deviation was plotted as a function of NIR-conPK11195 concentration (unchallenged (*circle*) or in the presence of 100 μM PK 11195 (*inverted triangle*)) or free NIR dye concentration (*square*); undosed cells (*diamond*) serve as a negative control for autofluorescence. $n = 3$ wells.

concentration for each of the three intensities scanned. The data presented in Fig. 3 were acquired at an intensity setting of ten; all wells incubated with NIR-conPK11195 concentrations greater than 70 nM were saturated under these conditions and could therefore not be accurately quantified. At the lower intensity settings, higher dosages were quantifiable while the lower concentrations were undetectable. The fluorescence intensity of the cells dosed with 100 nM to 1 μM NIR-conPK11195 increased dramatically as a function of concentration and was presumed to result from nonspecifically binding to the lipid membrane of the cells or perhaps another protein altogether (data not shown). While more studies are necessary to determine the exact cause of this increased cellular uptake or association under these conditions, the *in vitro* TSPO-specificity and *in vivo* contrast enhancement by NIR-conPK11195 accumulation demonstrated below suggest that the sub-micromolar binding affinity may be suitable for *in vivo* imaging. Previous results demonstrating the utility of NIR-conPK11195 for *in vivo* imaging of colonic tumors further support this claim [38].

In vivo imaging experiments were initiated approximately 3 weeks post-inoculation of the tumor cells. The normalized fluorescence images taken pre- and post-injection of NIR-conPK11195 and free NIR dye are shown in Fig. 4a, b for qualitative and quantitative visualization of the *in vivo* biodistribution, clearance and accumulation of the TSPO-targeted and non-targeted agents, respectively. Since these images are displayed on the same scale, a direct quantitative comparison can be made between the biodistribution profiles of free NIR dye and TSPO-targeted probe over time; this quantitative comparison is later discussed in terms of the time activity curves generated from ROI analyses. Prior to injection, the mice are essentially devoid of fluorescence, revealing the negligible autofluorescence of tissue in the exploited wavelength region. Approximately 1 h post-injection, both compounds exhibit fairly

uniform distribution throughout the mice. Over time, the free NIR dye clears primarily through the kidneys with a much more rapid clearance profile than NIR-conPK11195, which is cleared through both the renal and hepatobiliary systems. After four hours, NIR-conPK11195 preferentially accumulates in the tumor regions to a significantly greater extent than the free NIR dye ($p < 0.001$ from 4–48 h post-injection; quantification discussed below). This enhanced fluorescence signal in the MDA-MB-231 tumors of the mice injected with NIR-conPK11195 is consistent with our *in vitro* observations of conPK11195- and TSPO-specific cellular uptake of NIR-conPK11195 as well as literature precedence [33].

Images from the 48-h time point are depicted in Fig. 5, further illustrating the ability to discriminate tumor from normal tissue with the TSPO-targeted molecular imaging agent (a) over the free NIR dye (b). The tumor regions of the mice injected with free NIR dye (b) show some detectable fluorescence signal, presumably due to the enhanced permeability and retention effect [46]. However, the *in vivo* and harvested tumors of the mice injected with NIR-conPK11195 (a) are on average 5-fold more intense ($p < 0.001$) than the mice injected with free NIR dye (b), and maintain significant tumor to normal contrast enhancement from 4 to 48 h post-injection (quantification discussed below).

To statistically evaluate the ability of our TSPO-targeted NIR-conPK11195 agent to label MDA-MB-231 cells *in vivo*, the fluorescence intensity of the tumor and normal (muscle) tissue regions were quantified in terms of normalized fluorescence intensity to generate time activity curves. Two noticeably distinct clearance profiles for NIR-conPK11195 (tumor, circle and normal, inverted triangle) and free NIR dye (tumor, square and normal, diamond) are seen in Fig. 6a. More specifically, the time necessary to clear half of the maximum fluorescence intensity occurring at 10 min post-injection is ~10 h for the NIR-conPK11195, but
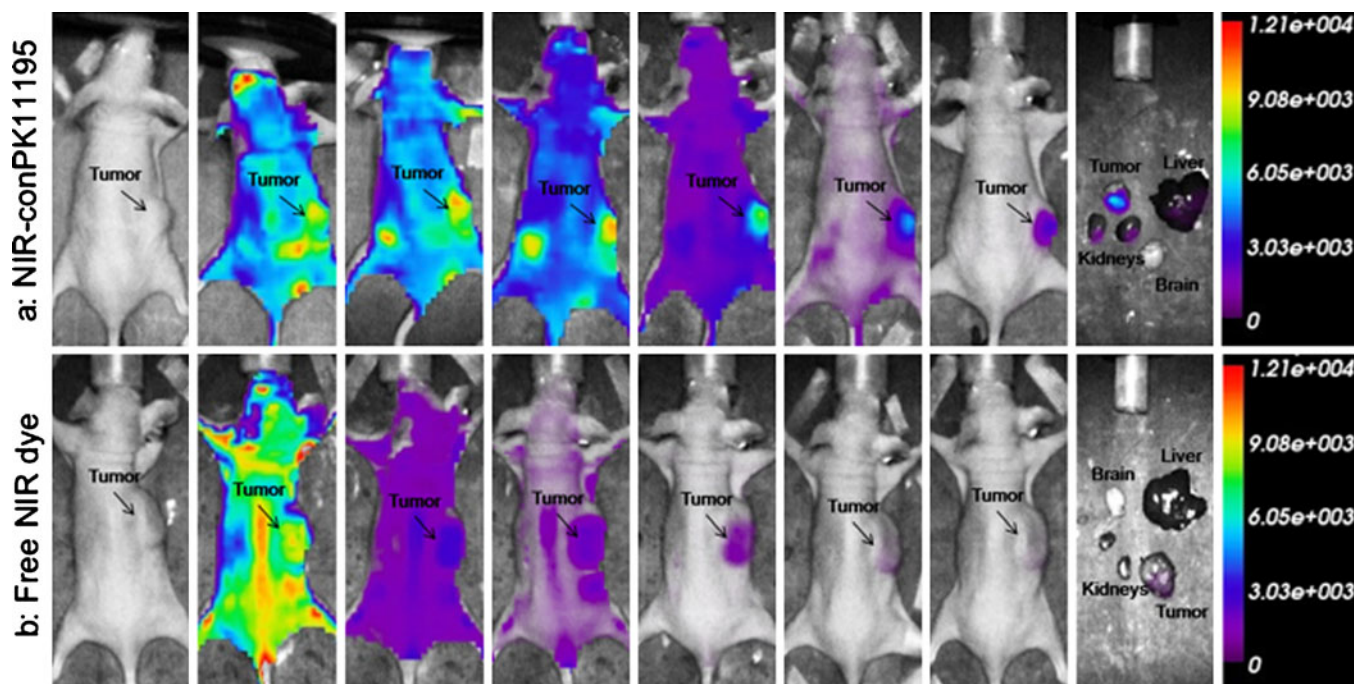
Fig. 4. Direct comparison of the biodistribution and accumulation of the TSPO-targeted NIR-conPK11195 (**a**) and free NIR dye (**b**) in tumor-bearing mice demonstrates significantly different clearance profiles and enhanced preferential labeling of MDA-MB-231 tumors *in vivo* by NIR-conPK11195. Fluorescence images were normalized to laser power and integration time, overlaid onto the corresponding white light images, and displayed in terms of normalized photon counts over 48 h post-injection (pi). Images are representative of *n*=3 mice per group. *Note:* These images are all displayed on the same scale (0 to 12,149 counts) pre-injection, 1, 4, 6, 12, 24, and 48 h pi (*left* to *right*).
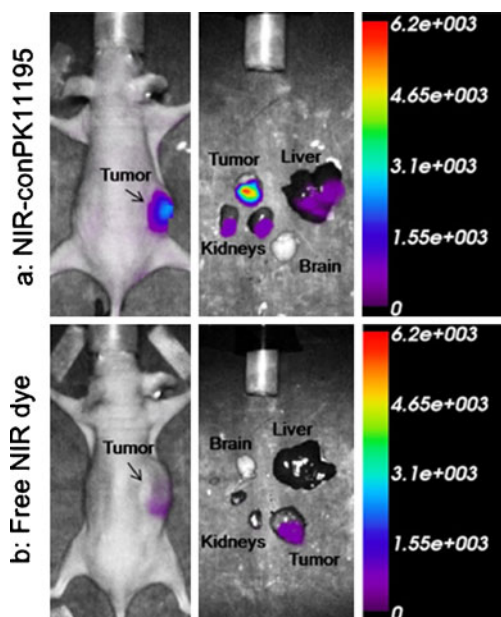

Fig. 5. NIR-conPK11195 preferentially labels MDA-MB-231 tumors *in vivo* and substantially enhances the tumor-associated signal over free NIR dye (see also Fig. 6). **a** and **b** Fluorescence overlays of MDA-MB-231 tumor-bearing mice and harvested tissues ~48 h pi of NIR-conPK11195 and free NIR dye, respectively. Representative of *n*=3 mice per group.

only ~3 h for the free NIR dye (estimated from Fig. 6a). We attribute the differences in $t_{1/2}$ primarily to the TSPO-targeting capabilities of NIR-conPK11195, which were clearly demonstrated in the *in vitro* competition assays (Fig. 3), and the polarity differences between the two agents. HPLC analysis indicates that free NIR dye is more hydrophilic than NIR-conPK11195 (data not shown), which should result in more rapid excretion from the blood stream.

Figure 6a also illustrates the significant accumulation of NIR-conPK11195 in the tumor (circle) relative to the normal muscle tissue (inverted triangle), as well as compared with the tumor (square) and normal (diamond) tissue of the mice injected with free NIR dye. This tumor-specific accumulation of NIR-conPK11195 can be quantitatively expressed in terms of two contrast ratios: (1) Tumor/normal ratio—the fluorescence intensity of the tumor regions relative to the normal regions of the tumor-bearing mice and (2) TSPO-targeted/free ratio—the average intensity of the tumors in mice injected with the TSPO-targeted agent (NIR-conPK11195) relative to the average intensity of the tumors in mice injected with the free NIR dye (Fig. 6b, c). The intensity in the tumor region due to accumulation of NIR-conPK11195 becomes significantly greater than the fluorescence intensity of the normal tissue 4 h post-injection ($p<0.001$), suggesting preferential labeling of MDA-MB-231 tumors *in vivo*. The contrast enhancement steadily increases to 11-fold at 48 h post-injection of the TSPO-targeted agent ($p<0.001$). Furthermore, conjugation of the PK 11195 analog (conPK11195) to the

a

b

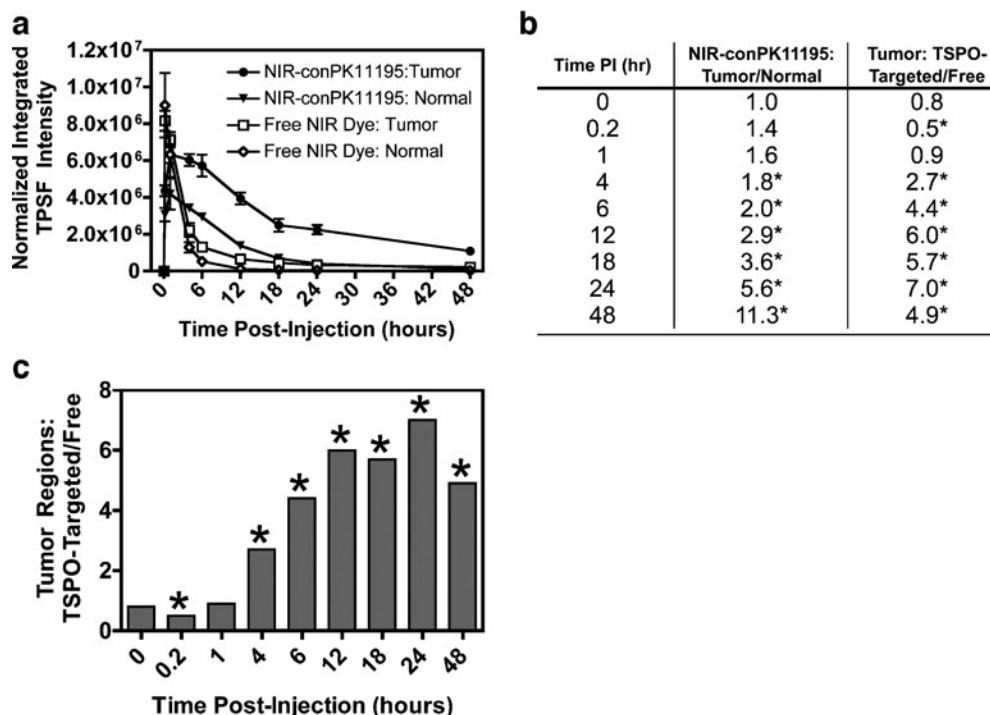| Time PI (hr)	NIR-conPK11195: Tumor/Normal	Tumor: TSPO-Targeted/Free
0	1.0	0.8
0.2	1.4	0.5*
1	1.6	0.9
4	1.8*	2.7*
6	2.0*	4.4*
12	2.9*	6.0*
18	3.6*	5.7*
24	5.6*	7.0*
48	11.3*	4.9*

c

Fig. 6. **a** Time-activity curves illustrate the distinct clearance profile of NIR-conPK11195 relative to free NIR dye, further demonstrate tumor specificity of NIR-conPK11195 *in vivo*, and reveal the significant signal enhancement resulting from the TSPO-targeted NIR molecular imaging probe. **b** ROI contrast ratios. **c** Graphical representation of the TSPO-targeted to free NIR dye ratio demonstrating significant fluorescence signal enhancement from the NIR-conPK11195 relative to the free NIR dye. *$p < 0.001$.

NIR dye provides a significant 3–7-fold contrast enhancement over the free NIR dye as demonstrated by the TSPO-targeted/free contrast ratio (Fig. 6b, c; $p < 0.001$). This substantial signal enhancement not only provides tumor specificity over compound pooling and functional information regarding the suspected lesion, but also may allow for detection of smaller and/or deeper tumors.

Discussion

Several approaches have been investigated for molecular imaging of breast cancer including [18F]FDG-PET measures of glucose metabolism [16–19], [18F]FLT-PET assessment of thymidine kinase-1 activity [20–23], and [18F]FES-PET evaluation of estrogen receptor expression [24–26]. These molecular imaging probes provide valuable functional information and have demonstrated some success in the management of breast cancer patients. However, novel molecular imaging techniques, such as the TSPO-targeted approach presented here, are necessary to assess the complexity and heterogeneity of breast cancer and to address the attendant difficulties associated with evaluating response(s) to increasingly personalized medicine. Furthermore, it is likely that important biomarkers or molecular responses are overlooked due to the narrow scope of existing imaging techniques. In order for the use of molecularly targeted therapy to become mainstream, the discovery, evaluation, and

validation of new imaging probes for innovative targets in cancer imaging will be required.

As a complementary approach to breast cancer imaging, our laboratory has developed molecular imaging agents that target the TSPO [39, 41, 43, 44, 47]. The TSPO is involved in a number of cellular processes and is upregulated in a variety of neurodegenerative diseases and cancers, including breast cancer [30–37]. A number of exogenous TSPO ligands and TSPO-targeted agents have been developed to non-invasively image these TSPO expression profiles [45, 48–54], but the majority of this work has primarily focused on nuclear imaging of neuroinflammation with radiolabeled PK 11195 [reviewed in [24]]. To date, the oncologic usages of TSPO-targeted tracers have been limited to cancers of the brain [31, 36] and colon [38]. Several other fluorescently-labeled TSPO-targeted agents have also been developed, but with the exception of the NIR-conPK11195 probe employed here, these agents have been used almost exclusively for *in vitro* screening only [39, 41–45].

In this study, we report the quantitative evaluation of our NIR-labeled TSPO-targeted probe (NIR-conPK11195) for *in vivo* molecular imaging of TSPO in breast cancer. Through fluorescence microscopy, we illustrate the internalization and intracellular labeling of TSPO-expressing MDA-MB-231 cells by NIR-conPK11195, but not free NIR dye. The lack of fluorescence in the cells dosed with unconjugated NIR dye suggests that the uptake of NIR-conPK11195 is

conPK11195 specific. In addition, the fluorescence overlay provides evidence that the fluorescent signal is emanating from the nuclear and perinuclear region of the NIR-conPK11195-dosed cells, as one would expect from the nuclear and mitochondrial location of TSPO in MDA-MB-231 cells [33]. The significant decrease in NIR-conPK11195 uptake in the presence of the known TSPO ligand PK 11195 in *in vitro* cellular uptake and competition assays validates the TSPO-specificity of NIR-conPK11195. Finally, the selective labeling of breast cancer cells *in vivo* by NIR-conPK11195 suggests the utility for *in vivo* molecular imaging of TSPO in breast cancer.

Conclusions

Here, we present the first study to demonstrate the feasibility of molecular imaging of TSPO expression in a pre-clinical model of breast cancer. Specifically, we report the effective use of a NIR-labeled TSPO-targeted probe for labeling of MDA-MB-231 human breast adenocarcinoma cells in an *in vivo* pre-clinical model and validate its dose-dependence and TSPO-specificity *in vitro*. Given the importance of molecular imaging in cancer detection, diagnosis and monitoring of disease as well as the impact of pre-clinical studies on therapeutic efficacy monitoring and drug discovery, we believe the molecular imaging of TSPO in breast cancer will be of value to both the molecular imaging and cancer research communities. Furthermore, this work represents a potentially translational methodology as radiolabeled PK 11195 has already been used in the clinic for imaging of neurodegenerative diseases.

References

1. American Cancer Society (2009) Cancer Facts and Figures. Atlanta: American Cancer Society
2. Elmore JG, Armstrong K, Lehman CD, Fletcher SW (2005) Screening for breast cancer. JAMA 293(10):1245–1256
3. Carney PA, Miglioretti DL, Yankaskas BC et al (2003) Individual and combined effects of age, breast density, and hormone replacement therapy use on the accuracy of screening mammography. Ann Intern Med 138(3):168–175
4. DeMartini W, Lehman C, Partridge S (2008) Breast MRI for cancer detection and characterization: a review of evidence-based clinical applications. Acad Radiol 15(4):408–416
5. Stavros AT, Thickman D, Rapp CL, Dennis MA, Parker SH, Sisney GA (1995) Solid breast nodules: use of sonography to distinguish between benign and malignant lesions. Radiology 196(1):123–134
6. Bremer C, Ntziachristos V, Weissleder R (2003) Optical-based molecular imaging: contrast agents and potential medical applications. Eur Radiol 13(2):231–243
7. Cerussi A, Shah N, Hsiang D, Durkin A, Butler J, Tromberg BJ (2006) *In vivo* absorption, scattering, and physiologic properties of 58 malignant breast tumors determined by broadband diffuse optical spectroscopy. J Biomed Opt 11(4)
8. Godavarty A, Thompson AB, Roy R et al (2004) Diagnostic imaging of breast cancer using fluorescence-enhanced optical tomography: phantom studies. J Biomed Opt 9(3):488–496
9. Intes X (2005) Time-domain optical mammography SoftScan: Initial results. Acad Radiol 12(8):934–947
10. Ntziachristos V, Chance B (2001) Probing physiology and molecular function using optical imaging: applications to breast cancer. Breast Cancer Res 3(1):41–46
11. Ntziachristos V, Yodh AG, Schnall M, Chance B (2000) Concurrent MRI and diffuse optical tomography of breast after indocyanine green enhancement. Proc Natl Acad Sci U S A 97(6):2767–2772
12. Tromberg BJ, Cerussi A, Shah N et al (2005) Imaging in breast cancer—diffuse optics in breast cancer: detecting tumors in pre-menopausal women and monitoring neoadjuvant chemotherapy. Breast Cancer Res 7(6):279–285
13. Kaijzel EL, van der Pluijm G, Lowik CWGM (2007) Whole-body optical imaging in animal models to assess cancer development and progression. Clin Cancer Res 13(12):3490–3497
14. Luker GD, Luker KE (2008) Optical imaging: current applications and future directions. J Nucl Med 49(1):1–4
15. Margolis DJ, Hoffman JM, Herfkens RJ, Jeffrey RB, Quon A, Gambhir SS (2007) Molecular imaging techniques in body imaging. Radiology 245(2):333–356
16. Dose Schwarz J, Bader M, Jenicke L, Hemminger G, Janicke F, Avril N (2005) Early prediction of response to chemotherapy in metastatic breast cancer using sequential 18F-FDG PET. J Nucl Med 46(7):1144–1150
17. Schelling M, Avril N, Nahrig J et al (2000) Positron emission tomography using [(18)F]fluorodeoxyglucose for monitoring primary chemotherapy in breast cancer. J Clin Oncol 18(8):1689–1695
18. Smith IC, Welch AE, Hutcheon AW et al (2000) Positron emission tomography using [(18)F]-fluorodeoxy-D-glucose to predict the pathologic response of breast cancer to primary chemotherapy. J Clin Oncol 18(8):1676–1688
19. Wahl RL, Zasadny K, Helvie M, Hutchins GD, Weber B, Cody R (1993) Metabolic monitoring of breast cancer chemohormonotherapy using positron emission tomography: initial evaluation. J Clin Oncol 11(11):2101–2111
20. Been LB, Elsinga PH, de Vries J et al (2006) Positron emission tomography in patients with breast cancer using (18)F-3′-deoxy-3′-fluoro-l-thymidine ((18)F-FLT)-a pilot study. Eur J Surg Oncol 32(1):39-43
21. Kenny L, Coombes RC, Vigushin DM, Al-Nahhas A, Shousha S, Aboagye EO (2007) Imaging early changes in proliferation at 1 week post chemotherapy: a pilot study in breast cancer patients with 3′-deoxy-3′-[18F]fluorothymidine positron emission tomography. Eur J Nucl Med Mol Imaging 34(9):1339–1347
22. Pio BS, Park CK, Pietras R et al (2006) Usefulness of 3′-[F-18]fluoro-3′-deoxythymidine with positron emission tomography in predicting breast cancer response to therapy. Mol Imaging Biol 8(1):36–42
23. Smyczek-Gargya B, Fersis N, Dittmann H et al (2004) PET with [18F] fluorothymidine for imaging of primary breast cancer: a pilot study. Eur J Nucl Med Mol Imaging 31(5):720–724
24. Jonson SD, Welch MJ (1998) PET imaging of breast cancer with fluorine-18 radiolabeled estrogens and progestins. Q J Nucl Med 42(1):8–17
25. Linden HM, Stekhova SA, Link JM et al (2006) Quantitative fluoroestradiol positron emission tomography imaging predicts response to endocrine treatment in breast cancer. J Clin Oncol 24(18): 2793–2799
26. Mankoff DA, Link JM, Linden HM, Sundararajan L, Krohn KA (2008) Tumor receptor imaging. J Nucl Med 49:149S–163S
27. Mankoff DA (2006) Radiotracer breast cancer imaging: beyond FDG and MIBI. Phys Med 21(Suppl 1):12–16
28. Pantaleo MA, Nannini M, Maleddu A et al (2008) Conventional and novel PET tracers for imaging in oncology in the era of molecular therapy. Cancer Treat Rev 34(2):103–121
29. Quon A, Gambhir SS (2005) FDG-PET and beyond: molecular breast cancer imaging. J Clin Oncol 23(8):1664–1673
30. Papadopoulos V, Baraldi M, Guilarte TR et al (2006) Translocator protein (18 kDa): new nomenclature for the peripheral-type benzodiazepine receptor based on its structure and molecular function. Trends Pharmacol Sci 27(8):402–409
31. Black KL, Ikezaki K, Toga AW (1989) Imaging of brain tumors using peripheral benzodiazepine receptor ligands. J Neurosurg 71(1):113–118
32. Han Z, Slack RS, Li W, Papadopoulos V (2003) Expression of Peripheral Benzodiazepine Receptor (PBR) in human tumors: relationship to breast, colorectal, and prostate tumor progression. J Recept Signal Transduct. 23(2–3):225–238

33. Hardwick M, Fertikh D, Culty M, Li H, Vidic B, Papadopoulos V (1999) Peripheral-type benzodiazepine receptor (PBR) in human breast cancer: correlation of breast cancer cell aggressive phenotype with PBR expression, nuclear localization, and PBR-mediated cell proliferation and nuclear transport of cholesterol. Cancer Res 59 (4):831–842

34. Hardwick M, Rone J, Han Z, Haddad B, Papadopoulos V (2001) Peripheral-type benzodiazepine receptor levels correlate with the ability of human breast cancer MDA-MB-231 cell line to grow in SCID mice. Int J Cancer 94(3):322–327

35. Maaser K, Grabowski P, Sutter AP et al (2002) Overexpression of the peripheral benzodiazepine receptor is a relevant prognostic factor in stage III colorectal cancer. Clin Cancer Res 8(10):3205–3209

36. Starosta-Rubinstein S, Ciliax BJ, Penney JB, McKeever P, Young AB (1987) Imaging of a glioma using peripheral benzodiazepine receptor ligands. Proc Natl Acad Sci U S A 84(3):891–895

37. Venneti S, Lopresti BJ, Wiley CA (2006) The peripheral benzodiazepine receptor (Translocator protein 18 kDa) in microglia: from pathology to imaging. Prog Neurobiol 80(6):308–322

38. Deane NG, Manning HC, Foutch AC et al (2007) Targeted imaging of colonic tumors in smad3−/− mice discriminates cancer and inflammation. Mol Cancer Res 5(4):341–349

39. Manning HC, Goebel T, Marx JN, Bornhop DJ (2002) Facile, efficient conjugation of a trifunctional lanthanide chelate to a peripheral benzodiazepine receptor ligand. Org Lett 4(7):1075–1078

40. Ma G, Gallant P, McIntosh L (2007) Sensitivity characterization of a time-domain fluorescence imager: eXplore Optix. Appl Opt 46 (10):1650–1657

41. Bai M, Wyatt SK, Han Z, Papadopoulos V, Bornhop DJ (2007) A novel conjugable translocator protein ligand labeled with a fluorescence dye for in vitro imaging. Bioconjug Chem 18(4):1118–1122

42. Kozikowski AP, Kotoula M, Ma D, Boujrad N, Tuckmantel W, Papadopoulos V (1997) Synthesis and biology of a 7-nitro-2,1,3-benzoxadiazol-4-yl derivative of 2-phenylindole-3-acetamide: a fluorescent probe for the peripheral-type benzodiazepine receptor. J Med Chem 40(16):2435–2439

43. Manning HC, Goebel T, Thompson RC, Price RR, Lee H, Bornhop DJ (2004) Targeted molecular imaging agents for cellular-scale bimodal imaging. Bioconjug Chem 15(6):1488–1495

44. Manning HC, Smith SM, Sexton M et al (2006) A peripheral benzodiazepine receptor targeted agent for in vitro imaging and screening. Bioconjug Chem 17(3):735–740

45. Taliani S, Simorini F, Sergianni V et al (2007) New fluorescent 2-phenylindolglyoxylamide derivatives as probes targeting the peripheral-type benzodiazepine receptor: design, synthesis, and biological evaluation. J Med Chem 50(2):404–407

46. Iyer AK, Khaled G, Fang J, Maeda H (2006) Exploiting the enhanced permeability and retention effect for tumor targeting. Drug Discov Today 11(17-18):812–818

47. Bai M, Rone MB, Papadopoulos V, Bornhop DJ (2007) A novel functional translocator protein ligand for cancer imaging. Bioconjug Chem 18(6):2018–2023

48. Benavides J, Quarteronet D, Imbault F et al (1983) Labelling of "peripheral-type" benzodiazepine binding sites in the rat brain by using [3H]PK 11195, an isoquinoline carboxamide derivative: kinetic studies and autoradiographic localization. J Neurochem 41(6):1744–1750

49. Chaki S, Funakoshi T, Yoshikawa R et al (1999) Binding characteristics of [3H]DAA1106, a novel and selective ligand for peripheral benzodiazepine receptors. Eur J Pharmacol 371(2–3):197–204

50. Ferzaz B, Brault E, Bourliaud G et al (2002) SSR180575 (7-chloro-N, N,5-trimethyl-4-oxo-3-phenyl-3,5-dihydro-4H-pyridazino[4,5-b]i ndole-1-acetamide), a peripheral benzodiazepine receptor ligand, promotes neuronal survival and repair. J Pharmacol Exp Ther 301(3):1067–1078

51. Newman AH, Lueddens HW, Skolnick P, Rice KC (1987) Novel irreversible ligands specific for "peripheral" type benzodiazepine receptors: (+/−)-, (+)-, and (−)-1-(2-chlorophenyl)-N-(1-methylpropyl)-N- (2-isothiocyanatoethyl)-3-isoquinolinecarboxamide and 1-(2-isothiocyanatoethyl)-7-chloro-1,3-dihydro-5-(4-chlorophenyl)-2H-1,4-benzodiazepin-2-one. J Med Chem 30(10):1901–1905

52. Okuyama S, Chaki S, Yoshikawa R et al (1999) Neuropharmacological profile of peripheral benzodiazepine receptor agonists, DAA1097 and DAA1106. Life Sci 64(16):1455–1464

53. Romeo E, Auta J, Kozikowski AP et al (1992) 2-Aryl-3-indoleacetamides (FGIN-1): a new class of potent and specific ligands for the mitochondrial DBI receptor (MDR). J Pharmacol Exp Ther 262(3):971–978

54. Vin V, Leducq N, Bono F, Herbert JM (2003) Binding characteristics of SSR180575, a potent and selective peripheral benzodiazepine ligand. Biochem Biophys Res Commun 310(3):785–790